Journal of the Korean Physical Society, Vol. 73, No. 11, December 2018, pp. 1703∼1707

Magnetic properties of $Mn_{54}Al_{46}C_{2.44}/Sm_2Fe_{17}N_3$ and $Mn_{54}Al_{46}C_{2.44}/Fe_{65}Co_{35}$ composites

Hui-Dong Qian, Ping-Zhan Si, Jung Tae Lim, Jong-Woo Kim, Jihoon Park* and Chul-Jin Choi†
Powder and Ceramic Division, Korea Institute of Materials Science, Changwon 51508, Korea

(Received 1 October 2018, in final form 16 October 2018)

Ferromagnetic τ-phase $Mn_{54}Al_{46}C_{2.44}$ particles were synthesized, and its composites with commercial $Sm_2Fe_{17}N_3$ and synthesized $Fe_{65}Co_{35}$ powders were fabricated. Smaller grain size than the single domain size of the $Mn_{54}Al_{46}C_{2.44}$ without obvious grain boundaries and secondary phases is the origin for the low intrinsic coercivity. It was confirmed that the magnetic properties of the $Mn_{54}Al_{46}C_{2.44}$ can be enhanced by magnetic exchange coupling with the hard magnetic $Sm_2Fe_{17}N_3$ and soft magnetic $Fe_{65}Co_{35}$. The high degrees of the exchange coupling were verified by calculating first derivative curves. Thermo-magnetic stabilities of the composites from 100 to 400 K were measured and compared. It was demonstrated that the $Mn_{54}Al_{46}C_{2.44}$ based composites containing $Sm_2Fe_{17}N_3$ and $Fe_{65}Co_{35}$ could be promising candidates for future permanent magnetic materials with the proper control of purity, magnetic properties, etc.

PACS numbers: 75.20.En, 75.50.Ww
Keywords: MnAl, Composite magnet, Exchange coupling
DOI: 10.3938/jkps.73.1703

I. INTRODUCTION

Theoretically, ferromagnetic τ-phase MnAl has magnetic moment of $2.4\mu_B$/f.u. [1,2] and magnetocrystalline anisotropy constant (K) of 1.5×10^6 J/m^3 [1, 2]. The theoretical magnetic moment is lower than that of the low temperature phase MnBi of $3.63\mu_B$/f.u., while the K is close to the experimental results of 1.3×10^6 J/m^3 [3], which was measured at 300 K. Nevertheless, the experimental intrinsic coercivity (H_{ci}) of high purity Mn-Al is much lower than Mn-Bi [2,4]. On the other hand, low purity Mn-Al with high percentage of secondary phases, such as equilibrium γ_2- and β phases, exhibit much increased H_{ci} [5] because the secondary phases act as pinning sites for magnetic domain walls. In order to achieve both high saturation magnetization (σ_s) and H_{ci}, magnetic materials must have not only single domain sized grains, but also highly oriented magnetic domains at zero applied magnetic field, *i.e.*, anisotropic magnetic grains. Highly textured/anisotropic magnetic grains of Mn-Al were obtained by Matsushita Electric Industrial Co., Ltd., in 1970s [6–10], and their best maximum energy product [$(BH)_{max}$] achieved was 9.2 MGOe [8]. However, no works has been reported that has obtained such a high $(BH)_{max}$ after their results.

Another way to improve magnetic properties is to realize magnetic exchange coupling between two or more phases [11]. It is noted that the exchange coupling makes use of the high magnetization from soft phase and the coercivity from hard phase. Therefore, it is possible to achieve large $(BH)_{max}$ with the rare-earth free or reduced rare-earth permanent magnetic materials by the exchange coupling. Magnetic exchange coupling between two phases has been extensively studied by producing composite magnets or depositing multi-phase thin films [12–20]. However, the results of the most composite magnets exhibit only partial exchange coupling, and the reports on Mn Al C based composite magnets are very rare. Therefore, in this paper, we report the magnetic properties and thermo-magnetic stabilities of $Mn_{54}Al_{46}C_{2.44}$ based composites with hard magnetic $Sm_2Fe_{17}N_3$ and soft magnetic $Fe_{65}Co_{35}$ for permanent magnet application.

II. EXPERIMENTAL PROCEDURE

The Mn-Al-C ingot was produced using high-frequency vacuum induction furnace in argon environment (purity 99.999%). High-purity manganese (Mn) and aluminum (Al) pieces and carbon (C) powder were melted and casted in an alumina mould. The composition of the Mn-Al-C was controlled to be $Mn_{54}Al_{46}C_{2.44}$, and the compositional deviation due to the volatility of Mn was minimized by melting and casting in less than 3 minutes. The produced alloy was then gas-atomized

*E-mail: jpark@kims.re.kr
†E-mail: cjchoi@kims.re.kr

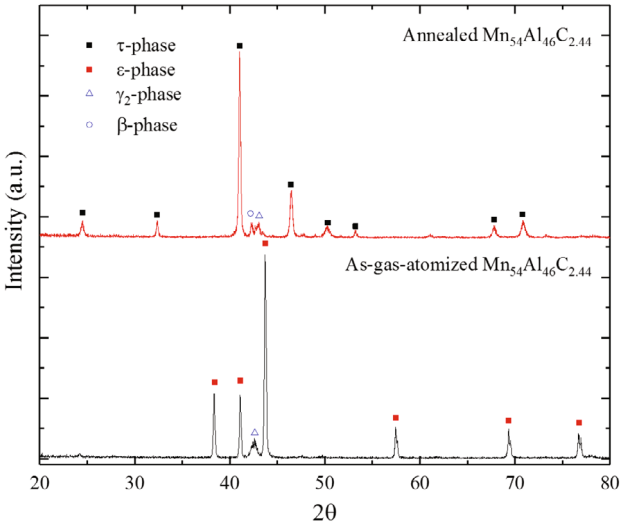

Fig. 1. (Color online) XRD patterns of the as-gas-atomized and annealed $Mn_{54}Al_{46}C_{2.44}$ particles.

using nitrogen gas at a pressure of 70 bar. The obtained powders were annealed at 500 °C for 20 minutes in argon environment to convert the hexagonal closed-packed paramagnetic ε-phase to tetragonal ferromagnetic τ-phase.

$Fe_{65}Co_{35}$ spherical chains were synthesized by reducing Fe^{2+} and Co^{2+}. Stoichiometric $FeCl_2{\cdot}4H_2O$ to $CoCl_2{\cdot}6H_2O$ ratio of 65 to 35 were dissolved in de ionized water, namely the solution A, followed by adding $NaBH_4$ dissolved solution, *i.e.*, the solution B, to the solution A. While the solution B was dropped into the solution A, the solution was magnetically stirred to produce uniform particle size and shape. Thereby, Fe and Co salts were reduced to crystalize α-phase $Fe_{65}Co_{35}$ metallic alloyed particles. The synthesized slush-like $Fe_{65}Co_{35}$ powder was washed with ethanol and collected by a permanent magnet for multiple times to remove residues. The black slush-like product was dried in a glove box.

The $Mn_{54}Al_{46}C_{2.44}/Sm_2Fe_{17}N_3$ and $Mn_{54}Al_{46}C_{2.44}/Fe_{65}Co_{35}$ composites were prepared by ultra-sonicating the mixtures of the powders in ethanol, followed by manual grinding in a mortar and pestle. The weight percent of the $Mn_{54}Al_{46}C_{2.44}$ powder was fixed to 70 wt.%, and $Sm_2Fe_{17}N_3$ or $Fe_{65}Co_{35}$ powder weight percent is controlled to 30 wt.%. It is noted that the $Sm_2Fe_{17}N_3$ powder was purchased from Sumitomo Corporation Japan.

The crystalline phases of the $Mn_{54}Al_{46}C_{2.44}$, $Sm_2Fe_{17}N_3$, and $Fe_{65}Co_{35}$ powders and their composites were identified with X-ray diffraction (XRD) with Cu-$K\alpha$ radiation. A physical property measurement system (PPMS) was used to characterize their magnetic properties. The particle size and size distribution were determined using transmission electron microscopy (TEM) and scanning electron microscope (SEM).

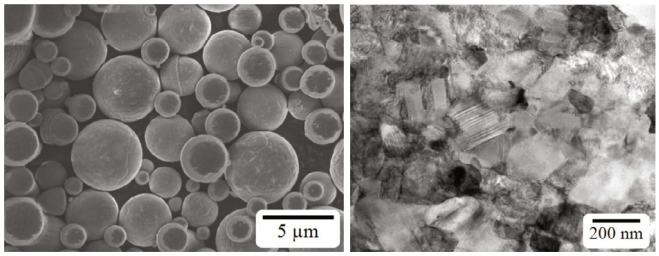

(a) (b)

Fig. 2. (a) SEM image and (b) TEM micrograph of the synthesized $Mn_{54}Al_{46}C_{2.44}$ particles.

III. RESULTS AND DISCUSSION

The XRD patterns of the as-gas-atomized and annealed $Mn_{54}Al_{46}C_{2.44}$ powders are shown in Fig. 1. Majority of the as-gas-atomized $Mn_{54}Al_{46}C_{2.44}$ powders appears to be the high temperature hexagonal closed-packed paramagnetic ε-phase, while small amount of secondary phase, γ_2-phase, still exist. The XRD pattern of the annealed powder exhibits mostly metastable τ phase and small amount of γ_2- and β phases. Figure 2 shows the morphology and microstructure of the obtained τ-phase $Mn_{54}Al_{46}C_{2.44}$ particles. Figure 2(a) indicates that the particle sizes of the τ-phase $Mn_{54}Al_{46}C_{2.44}$ are from 0.25 to 5 μm, and their grain sizes ranges from 10 to 200 nm as seen in Fig. 2(b).

Based on the XRD patterns in Fig. 1, we have calculated the average grain size using the Scherrer equation. The Scherrer equation is written as [21]:

$$\tau = \frac{K\lambda}{\beta \cos\theta},$$

where τ is the mean size of the grains, K is a dimensionless shape factor, λ is the X-ray wavelength, β is the line broadening at half the maximum intensity (FWHM), and θ is the Bragg angle. K varies with the shape of the crystallite; 0.89 for spherical and 0.94 for cubic particles, but its typical value is about 0.9 for unknown shape. We have used the XRD with Cu-$K\alpha$ radiation, therefore, the λ is 0.154 nm. Our calculations lead to the τ of 35.6 nm for as-gas-atomized powder and 37.7 nm for annealed powder. This result proves that the annealing at 500 °C for 20 min does not increase the mean size of the ordered domains/grain sizes. In order to achieve high H_{ci}, the grain size must be close to the single domain size of about 710 nm [22], and grains must be separated from each other. The synthesized τ-phase $Mn_{54}Al_{46}C_{2.44}$ particles, however, consist of numerous grains mostly ranging from 10 nm to 200 nm, and the grains have direct contact with neighboring grains as seen in Fig. 2(b). It is noted that the slightly prolonged annealing of the τ phase $Mn_{54}Al_{46}C_{2.44}$ may possibly cause the increased grain size and minor decomposition into the equilibrium γ_2- and β phases, *i.e.*, enhanced H_{ci}, but at the same time, results in decreased magnetization.

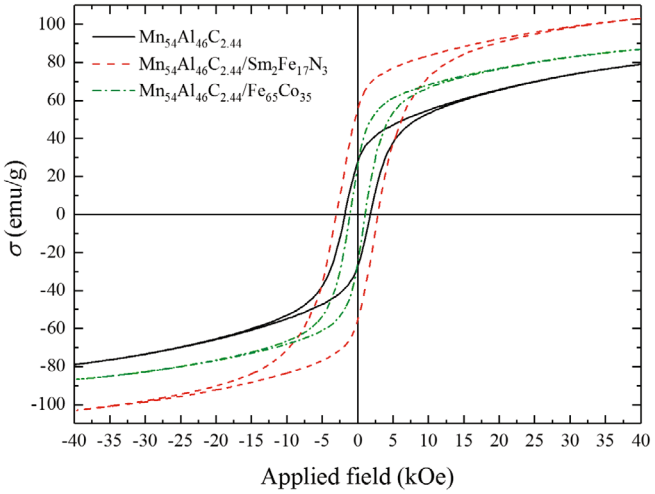

Fig. 3. (Color online) Magnetic hysteresis loops of the $Mn_{54}Al_{46}C_{2.44}$, $Mn_{54}Al_{46}C_{2.44}/Sm_2Fe_{17}N_3$, and $Mn_{54}Al_{46}C_{2.44}/Fe_{65}Co_{35}$ composites.

By producing composites of two or more magnetic materials, it is possible to optimize the σ_s and H_{ci} [20], *i.e.*, $(BH)_{max}$. We have fabricated composites of $Mn_{54}Al_{46}C_{2.44}$ with hard magnetic $Sm_2Fe_{17}N_3$ and soft magnetic $Fe_{65}Co_{35}$, and measured magnetic hysteresis loops for σ_s, remanent magnetization (σ_r), and H_{ci}. The exchange coupling between two phases occurs only if the thickness of soft phase is thinner than twice of the hard phase's domain wall thickness ($2\delta_w$) [11]. The experimental δ_w of Mn-Al is 15 nm [23]. The particle size of the $Sm_2Fe_{17}N_3$ varies from 100 nm to 1 μm and the diameter of the synthesized $Fe_{65}Co_{35}$ particle is 40 nm in average, which are greater than $2\delta_w$ (30 nm) of τ-phase Mn-Al. Since the $Sm_2Fe_{17}N_3$ or $Fe_{65}Co_{35}$ particles can be compacted between the $Mn_{54}Al_{46}C_{2.44}$ particles, the maximum range of magnetic exchange coupling is 60 nm in theory. Therefore, it can be estimated that the $Sm_2Fe_{17}N_3$ particles are only partially involved in exchange coupling, while the $Fe_{65}Co_{35}$ particles are fully involved in exchange coupling in ideal case.

The magnetic hysteresis loops of the $Mn_{54}Al_{46}C_{2.44}$, $Mn_{54}Al_{46}C_{2.44}/Sm_2Fe_{17}N_3$, and $Mn_{54}Al_{46}C_{2.44}/Fe_{65}Co_{35}$ composites are shown in Fig. 3. The maximum magnetic applied field was 4 T for all the measurements. The σ_s, σ_r, and H_{ci} of the $Mn_{54}Al_{46}C_{2.44}$ were measured to be 78.9 emu/g, 27.4 emu/g, and 1792 Oe, respectively, and those of the composites were changed according to the magnetic properties of the $Sm_2Fe_{17}N_3$ and $Fe_{65}Co_{35}$. The σ_s of the single phase $Sm_2Fe_{17}N_3$ and $Fe_{65}Co_{35}$ were 144.7 emu/g and 104.2 emu/g, respectively, while the H_{ci} were 4540 Oe and 350 Oe. It is noted that the σ_s of the synthesized $Fe_{65}Co_{35}$ is much lower than 240 emu/g of its bulk value [24]. This is attributed to the thermal agitation of magnetic spins on the surface of the particles, slight oxidation of $Fe_{65}Co_{35}$ particle or incomplete reduction of Fe- and Co-salts. Since the σ_s of the $Sm_2Fe_{17}N_3$ and $Fe_{65}Co_{35}$ are higher than the $Mn_{54}Al_{46}C_{2.44}$, the σ_s of the composites were increased to 103.1 emu/g and 86.9 emu/g, respectively, from 78.9 emu/g. However, the σ_r of the $Mn_{54}Al_{46}C_{2.44}/Fe_{65}Co_{35}$ composite was slightly decreased to 26.0 emu/g from 27.4 emu/g, while it was increased to 55.2 emu/g for $Mn_{54}Al_{46}C_{2.44}/Sm_2Fe_{17}N_3$ composite. The H_{ci} of the $Mn_{54}Al_{46}C_{2.44}/Sm_2Fe_{17}N_3$ and $Mn_{54}Al_{46}C_{2.44}/Fe_{65}Co_{35}$ composites were 3014 Oe and 1092 Oe, respectively.

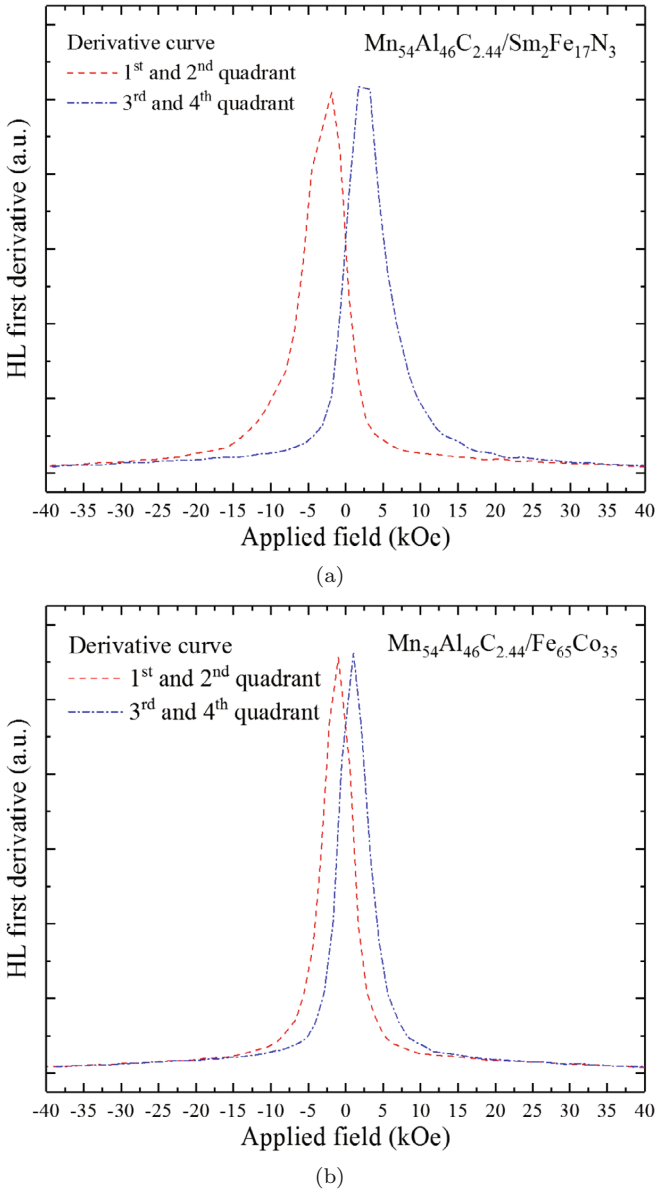

Fig. 4. (Color online) First derivatives of the magnetic hysteresis loops for the (a) $Mn_{54}Al_{46}C_{2.44}/Sm_2Fe_{17}N_3$ and (b) $Mn_{54}Al_{46}C_{2.44}/Fe_{65}Co_{35}$ composites.

In order to confirm the levels of the exchange coupling for the composites, first derivative curves in Fig. 4 were calculated from the magnetic hysteresis loops in Fig. 3. A

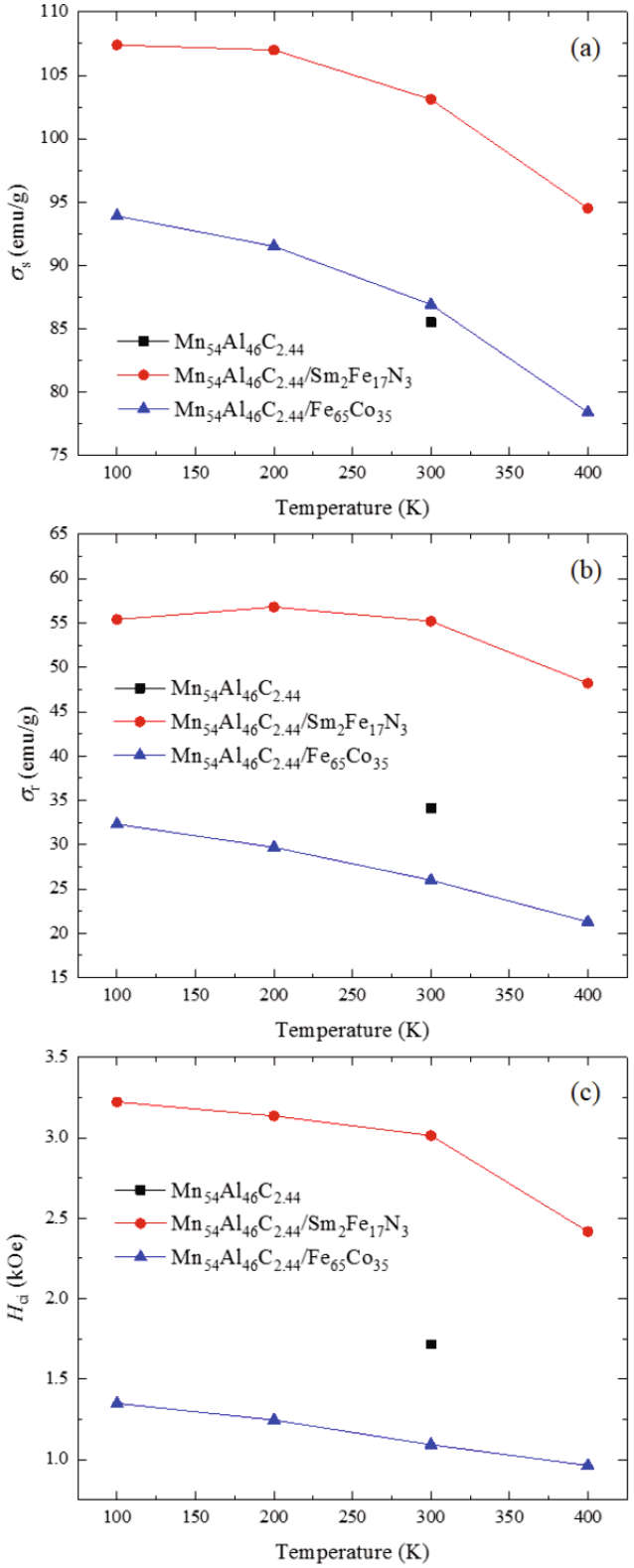

Fig. 5. (Color online) Temperature dependence of (a) saturation magnetization (σ_s), (b) remanent magnetization (σ_r), and (c) intrinsic coercivity (H_{ci}) of the $Mn_{54}Al_{46}C_{2.44}/Sm_2Fe_{17}N_3$ and $Mn_{54}Al_{46}C_{2.44}/Fe_{65}Co_{35}$ composites from 100 to 400 K. For comparison σ_s, σ_r, and H_{ci} of the single phase $Mn_{54}Al_{46}C_{2.44}$ at 300 K is also shown.

kink in the demagnetization curve of magnetic hysteresis loop indicates decoupling between the two phases. However, it is very difficult to observe a kink with naked eyes in many cases unless the kink is obvious. The derivative curves of the demagnetization curves, such as Fig. 4, can clearly demonstrate the no existence of a kink. Based on Fig. 4, both $Mn_{54}Al_{46}C_{2.44}/Sm_2Fe_{17}N_3$ and $Mn_{54}Al_{46}C_{2.44}/Fe_{65}Co_{35}$ composites are well exchange coupled without a kink in both derivative curves of the 1st and 2nd quadrants and 3^{rd} and 4^{th} quadrants.

Thermo-magnetic stabilities of the $Mn_{54}Al_{46}C_{2.44}/Sm_2Fe_{17}N_3$ and $Mn_{54}Al_{46}C_{2.44}/Fe_{65}Co_{35}$ composites were verified by measuring temperature dependence of magnetic hysteresis loops from 100 to 400 K, and their σ_s, σ_r, and H_{ci} are plotted in Figs. 5(a), (b), and (c). The σ_s, σ_r, and H_{ci} of the composites are 107.4 emu/g, 55.4 emu/g, and 3222 Oe, respectively, for $Mn_{54}Al_{46}C_{2.44}/Sm_2Fe_{17}N_3$ and 93.9 emu/g, 32.3 emu/g, and 1349 Oe for $Mn_{54}Al_{46}C_{2.44}/Fe_{65}Co_{35}$ at 100 K. These values gradually decrease by increasing temperature, therefore, reaching 94.5 emu/g, 48.2 emu/g, and 2417 Oe for $Mn_{54}Al_{46}C_{2.44}/Sm_2Fe_{17}N_3$ and 78.4 emu/g, 21.3 emu/g, and 963 Oe for $Mn_{54}Al_{46}C_{2.44}/Fe_{65}Co_{35}$ at 400 K. The temperature coefficients of σ_s, σ_r, and H_{ci}, *i.e.*, $\alpha_s = \Delta\sigma_s/\sigma_s$, $\alpha_r = \Delta\sigma_r/\sigma_r$, and $\beta = \Delta H_{ci}/H_{ci}$, are -0.040, -0.043, and -0.083%/K, respectively, for $Mn_{54}Al_{46}C_{2.44}/Sm_2Fe_{17}N_3$ and -0.055, -0.114, and -0.095%/K for $Mn_{54}Al_{46}C_{2.44}/Fe_{65}Co_{35}$. One interesting point is that the σ_r of the $Mn_{54}Al_{46}C_{2.44}/Sm_2Fe_{17}N_3$ slightly increases at 200 K due to the enhanced squareness in the demagnetization curve as seen in Fig. 5 (b).

IV. CONCLUSION

We have synthesized ferromagnetic τ-phase $Mn_{54}Al_{46}C_{2.44}$ particles using gas atomization process, and fabricated its composites with commercial $Sm_2Fe_{17}N_3$ and chemically synthesized $Fe_{65}Co_{35}$ powders. The first derivative curves of the demagnetization curves prove that the magnetic exchange coupling was well occurred between the two phases. The saturation magnetizations and intrinsic coercivities of the composites monotonically decrease with increasing temperature, while the remanent magnetization initially increases until 200 K due to enhanced squareness in the demagnetization curve.

ACKNOWLEDGMENTS

This research was supported by Future Materials Discovery Program through the National Research Foundation of Korea (NRF) funded by the Ministry of Science and ICT (2016M3D1A1027835).

REFERENCES

[1] A. Sakuma, J. Phys. Soc. Jpn. **63**, 1422 (1993).
[2] J. H. Park, Y. K. Hong, S. Bae, J. J. Lee, J. Jalli, G. S. Abo, N. Neveu, S. G. Kim, C. J. Choi and J. G. Lee, J. Appl. Phys. **107**, 09A731 (2010).
[3] T. Chen and W. E. Stutius, IEEE Trans. Magn. **10**, 581 (1974).
[4] S. M. Kim, H. J. Moon, H. B. Jung, S. M. Kim, H. S. Lee, H. I. Choi-Yim and W. Y. Lee, J. All. Comp. **708**, 1245 (2017).
[5] J. G. Lee, P. Li, C. J. Choi and X. L. Dong, This Solid Films **519**, 81 (2010).
[6] H. Yamamoto, U. S. Patent US3, 661, 567, (9 May 1972).
[7] T. Ohtani, N. Kato, S. Kojima, Y. Sakamoto, M. Tsukahara, K. Kojima, I. Konno and T. Kubo, U. S. Patent US3, 944, 445, (16 March 1976).
[8] T. Kubo, T. Ohtani, S. Kojima, N. Kato, K. Kojima, Y. Sakamoto, I. Konno and M. Tsukahara, U. S. Patent US3, 976, 519, (24 August 1976).
[9] Y. Sakamoto, N. Kato and T. Ohtani, U. S. Patent US4, 051, 706, 4 October 1977.
[10] T. Ohtani, N. Kato, S. Kojima, K. Kojima, Y. Sakamoto, I. Konno, M. Tsukahara and T. Kubo, IEEE Trans. Magn. **MAG-13**, 1328 (1977).
[11] E. F. Kneller and R. Hawig, IEEE Trans. Magn. **27**, 3588 (1991).
[12] Y. Liu, A. George, R. Skomski and D. J. Sellmyer, Appl. Phys. Lett. **99**, 172504 (2011).
[13] H. Zeng, S. Sun, J. Li, Z. L. Wang and J. P. Liu, Appl. Phys. Lett. **85**, 792 (2004).
[14] B. Ma, H. Wang, H. Zhao, C. Sun, R. Acharya and J. P. Wang, J. Appl. Phys. **109**, 083907 (2011).
[15] M. Marinescu, J. F. Liu, M. J. Bonder and G. C. Hadjipanayis, J. Appl. Phys. **103**, 07E120 (2008).
[16] C. W. Kim, Y. H. Kim, H. G. Cha, J. C. Kim and Y. S. Kang, Mol. Cryst. Liq. Cryst. **472**, 155 (2007).
[17] Y. Shen, Y. He, M. Q. Huang, D. Lee, S. Bauser, A. Higgins, C. Chen and S. Liu, J. Appl. Phys. **99**, 08B520 (2006).
[18] D. Wang, N. Poudyal, C. Rong, Y. Zhang, M. J. Kramer and J. P. Liu, J. Magn. Magn. Mater. **324**, 2836 (2012).
[19] N. V. Rama Rao, A. M. Gabay and G. C. Hadjipanayis, IEEE Trans. Magn. **49**, 3255 (2013).
[20] J. H. Park, Y. K. Hong, W. C. Lee, S. G. Kim, C. Rong, N. Poudyal, J. P. Liu and C. J. Choi, Scientific Reports **7**, 4960 (2017).
[21] A. L. Patterson, Phys. Rev. **56**, 978 (1939).
[22] T. Klemmer, D. Hoydick, H. Okumura, B. Zhang and W. A. Soffa, Scripta. Metall. Mater. **33**, 1793 (1995).
[23] G. F. Korznikova, J. Microsc. **239**, 239 (2010).
[24] C. W. Chen, J. Appl. Phys. **32**, S348 (1961).